Energy 278 (2023) 127888

Contents lists available at ScienceDirect

Energy

journal homepage: www.elsevier.com/locate/energy

Few layers graphene-based electrocatalysts for ORR synthesized by electrochemical exfoliation methods

C.D. Jaimes-Paez [a], E. Morallón [a,*], D. Cazorla-Amorós [b]

[a] Departamento de Química Física, Instituto Universitario de Materiales de Alicante (IUMA), University of Alicante, Ap. 99, 03080, Alicante, Spain
[b] Departamento de Química Inorgánica, Instituto Universitario de Materiales de Alicante (IUMA), University of Alicante, Ap. 99, 03080, Alicante, Spain

ARTICLE INFO

Keywords:
Platinum nanoparticles
Electrochemical exfoliation
Few layer graphene
ORR
HER

ABSTRACT

Graphene-based materials were synthesized by electrochemical exfoliation method (cathodic method) starting from a graphite sheet. In the established methodology, an initial immersion in H_2SO_4 was applied, followed by cathodic expansion in potassium sulphate, where the effect of the applied voltage was studied. Finally, by ultrasound treatment, the exfoliation was achieved to produce a dispersion of few layer graphene material. Once the optimum procedure was established, Pt nanoparticles were incorporated using $H_2PtCl_6.6H_2O$. This incorporation was studied at each stage of the graphene-based material synthesis to determine which was the most adequate to obtain the highest Pt dispersion and the best distribution of the Pt nanoparticles. In this sense, the incorporation of Pt in the graphene-based material colloidal dispersion by stirring for 3 h and sonication for 1 h, results in Pt nanoparticles with an average size of around 1 nm with an excellent distribution in the carbon material. The performance of this catalyst was compared with the commercial Pt/C electrocatalyst, showing a great oxygen reduction reaction (ORR) and hydrogen evolution reaction (HER) activity, exceeding it by far when comparing the mass-specific activity (A g_{Pt}^{-1}) In addition, it presents excellent stability and selectivity toward the 4-electron pathway in ORR, which is the most energy-efficient, and using half of the platinum loading compared to the commercial material.

1. Introduction

One of the greatest challenges of this century is to obtain energy from renewable resources due to the rapid growth in global energy consumption and the pollution and limited resources related to the use of fossil fuels [1–3]. Hydrogen is one of the most abundant elements on Earth and is considered one of the most promising fuels of the future to be used as a renewable and clean energy source, but it is not found in its pure state in the environment, so its production is of vital importance in global energy development [4–6]. The need to replace combustion engines has led to the development of promising new technologies like fuel cells that require the use of electrocatalytic materials and in which carbon nanomaterials play an essential role [3].

Graphene -based materials has grown so quickly due to their characteristics, since the experimentally measured properties have exceeded those obtained by any other material, and some have reached the theoretically predicted limits [7–14]. The development of scalable methods to produce large, processable amounts of high-quality graphene-based materials is essential to bridge the gap between laboratory studies and commercial applications [15]. However, more than a decade of research in graphene production has taught us that no single method can produce graphene in the expected quantity and quality, and therefore it is necessary to use different methods [8].

Different preparation procedures are detailed in the literature, but most cannot produce single-layer graphene sheets, and generally toxic waste is generated [16]. These techniques are also time consuming and sometimes involve high temperature operations [17–20].

The production of graphene-based materials by electrochemical exfoliation of graphite is a simple, cost-effective and environmentally friendly method for the large-scale production of high-quality graphene-based materials [7,21–27]; the method takes advantage of the electrical conductivity of graphite and consists of applying a potential difference between a graphite anode and/or cathode in the presence of an electrolyte to produce electrochemical intercalation or insertion of ions between the graphene sheets, increasing the interlayer space and facilitating delamination to obtain graphene [17,23,25]. The advantages of the cathodic exfoliation method include the absence of strong oxidizing conditions, thus minimizing the generation of structural defects and a

* Corresponding author.
E-mail address: morallon@ua.es (E. Morallón).

https://doi.org/10.1016/j.energy.2023.127888
Received 13 November 2022; Received in revised form 10 April 2023; Accepted 18 May 2023
Available online 19 May 2023

large amount of oxygen functional groups [15,26–30].

Otherwise, fuel cells powered by hydrogen from secure and renewable sources are the ideal solution for non-polluting vehicles [31]. The oxygen reduction reaction (ORR) is a fundamental process in electrochemistry and its slow kinetics is undoubtedly one of the main drawbacks for the large-scale commercialization of fuel cell technology [32–34].

Moreover, the hydrogen evolution reaction (HER) is of both fundamental and practical interest in the generation of green hydrogen in the electrolyzers. In recent decades, HER has attracted even more attention due to the increasing demand for renewable energy and the possibility of obtaining green energy from these renewable resources [35]. It is well known that Pt-based electrocatalysts have excellent HER performance with an overpotential close to zero [35]. The free energy of adsorption of H on Pt is close to the thermoneutral state ($\Delta G_{H^*} \approx 0$) [35–39]. This is the reason why Pt is considered the best HER electrocatalyst [35,37]. Noble metals have the best catalytic behavior towards HER; however, it is mandatory to reduce costs due to the high price of noble metals. A promising alternative is to use them in smaller quantities and increase their surface area so that their electrocatalytic behavior is not affected.

Graphene layers are chemically inert because the sp^2 carbon atoms in the basal plane have a uniform charge distribution and there are no efficient charge transfer points; this makes that bending of the graphene layer alters the charge distribution and results in enhanced electrochemical activity [35,40,41]. The development of composite materials that include graphene-based materials as support and metal nanoparticles with high activity can result in ideal candidates for their use as electrocatalysts in HER and ORR [23,40,42–45].

The synthesis of graphene-based materials by electrochemical exfoliation and the subsequent incorporation of metallic nanoparticles has been previously studied [23]; nevertheless, the graphene material obtained, by this method and other methods frequently used, has a high degree of oxidation, which negatively affects the electrical conductivity and consequently its electrocatalytic behavior [46,47]. On the other hand, the incorporation of Pt nanoparticles can be achieved, with a good particle distribution, although the particle size is close to 10 nm [23]. It is important to optimize the preparation method to reach smaller nanoparticle sizes, that permit to have high catalytic activity without the need of adding large amounts of Pt. Other studies have examined the performance of graphene-based electrocatalysts containing metal nanoparticles towards HER with excellent results; however, the catalytic activity does not surpass the commercial material Pt/C with a high Pt loading [36,48].

In this study, we propose the use of a high-quality graphene-based material synthesized by electrochemical method, through cathodic expansion, generating a few layers graphene material with a very low degree of oxidation, thus avoiding additional reduction steps, for its use as support of Pt nanoparticles. The Pt nanoparticles have been incorporated by a simple and straightforward method of stirring for 3 h and successive sonication for 1 h. The electrocatalyst obtained consists of 1 nm size Pt nanoparticles well distributed in the graphene-based material with an excellent catalytic activity to ORR and HER compared with a commercial Pt/C catalyst. In addition, the electrocatalyst has an outstanding resistance to CO poisoning, which represents an interesting alternative to commercial material.

2. Experimental

2.1. Materials and reagents

Materials and reagents used were Graphite flexible foil (Papyex 1980, obtained from Mersen), sulfuric acid (H_2SO_4) (PanReac AppliChem, 95–98%), potassium sulphate (K_2SO_4) (Sigma Aldrich, for analysis), potassium hydroxide (KOH) (VWR Chemicals, 85%), ethanol (C_2H_5OH) (Alfa Aesar, 99.5%), 2-propanol ($(CH_3)_2CHOH$) (Sigma Aldrich, for analysis), Nafion® 5% w/w (Sigma Aldrich), 20 wt% Pt/C (Sigma-Aldrich, 98%), hexachloroplatinic acid hexahydrate ($H_2PtCl_6.6H_2O$) (Sigma Aldrich) and sodium borohydride ($NaBH_4$) (Sigma Aldrich, 98%). All solutions were prepared using ultrapure water (18 MΩ cm, Millipore® Milli-Q® water). N_2 (99.999%), O_2 (99.995%) and H_2 (99.999%) were provided by Carburos Metálicos.

2.2. Synthesis procedure

2.2.1. Synthesis of graphene-based material by electrochemical exfoliation

Fig. 1 shows a scheme of the experimental procedure used for the preparation of graphene-based materials. The synthesis of graphene-based material was performed by cathodic expansion of a graphite foil with dimensions of 55 × 30 × 0.5 mm, after an initial immersion in 50 ml H_2SO_4 (95–98%) [49], leaving an area of the sheets without immersion for easy handling and electrical connection (step 1 in Fig. 1). The immersion time was between 0 and 72 h at room temperature. The graphite sheet obtained from the immersion was washed with plenty of ultrapure water to remove excess of H_2SO_4. Then, the obtained material was subjected to an electrochemical expansion step during 1 h, and two voltages (i.e., 10 and 15 V) were studied (step 2 in Fig. 1). For the electrochemical expansion, a two-electrode system was employed in which the graphite sheet was used as cathode and a platinized titanium mesh as anode placed parallel to the graphite sample at a distance of about 2 cm. 100 ml of 0.1 M K_2SO_4 solution was used as electrolyte (Fig. 1). After the electrochemical treatment, the expanded graphite sheet obtained and the pieces detached in the electrolyte were washed and filtered with abundant ultrapure water. Then, these materials were dispersed in a 100 ml ultrapure water-isopropanol (80/20) solution and subjected to a sonication step (step 3 in Fig. 1). The sonication stage was performed during 30 min with a sonicator using 50% of the power of the equipment (Q125 sonicator, obtained from Qsonica, Power: 125 Watts. Frequency: 20 kHz, Probe of 3 mm). The obtained dispersion was centrifuged at 4000 rpm for 10 min. From this process, the precipitated solid was taken which was dispersed again in 100 ml of ultrapure water/isopropanol (80/20). The sonication and centrifugation processes were repeated in some samples as indicated in Table 1 under the same conditions. Finally, a new sonication step was carried out under the same conditions, and the dispersion was subjected to the centrifugation step at 1300 rpm for 10 min, where the supernatant was taken this time to finally obtain the dispersed graphene material (step 4 in Fig. 1). Table 1 shows the conditions used for the synthesis of the different graphene-based materials and the nomenclature for the samples (Gr-X).

2.2.2. Incorporation of Pt nanoparticles

The incorporation of Pt nanoparticles has been performed on selected graphene-based material dispersions using $H_2PtCl_6.6H_2O$ as Pt precursor. The precursor of platinum has been incorporated at different steps of the preparation process to identify in which step a better incorporation occurs: i) in the initial immersion with H_2SO_4(c) (denoted as Gr-X/Pt–I), ii) in the electrolyte used in the electrochemical cathodic expansion (denoted as Gr-X/Pt-E) and iii) in the obtained dispersions of graphene-based material; in this case, the incorporation was performed by stirring for 3 h followed by a bath sonication stage for 1 h. In this last case, the addition of $NaBH_4$ has also been studied (denoted as Gr-X/Pt–S-R in presence of $NaBH_4$ and Gr-X/Pt–S without $NaBH_4$). In addition, the effect of the sonication step was studied and a sample without the addition of reducing agent and without sonication has been studied (denoted as Gr-X/Pt-S-NS). When the addition of $NaBH_4$ was made, this was done by adding 100 μl of $NaBH_4$ with a concentration of 1.5 M and after 45 min in 10 mL of graphene-based dispersion, the system was sonicated in a bath for 2 min and then centrifugated at 5000 rpm. After that, the supernatant was taken and redispersed in 50 ml of water/isopropanol 80/20 solution. For the calculations of the volume of the $H_2PtCl_6.6H_2O$ solution to be incorporated to obtain a final 10 wt% of platinum in the graphene material, the concentration of graphene material obtained from the synthesis method at conditions that produce the

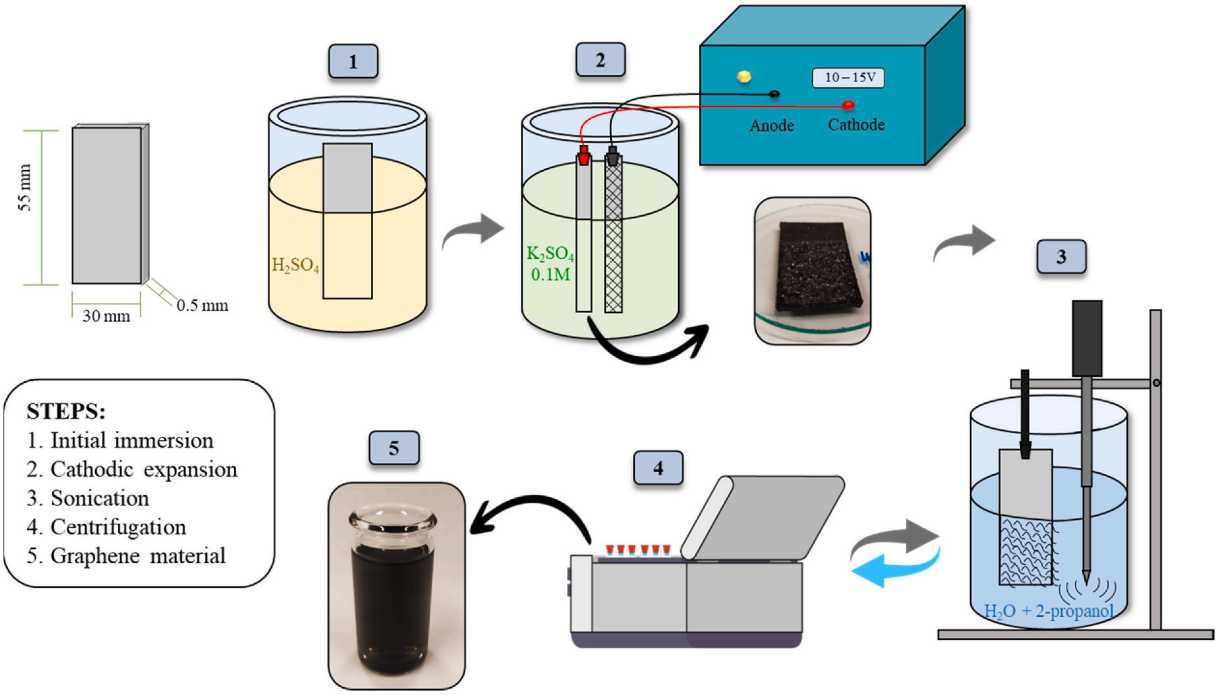

Fig. 1. Experimental scheme for the synthesis of dispersed graphene material.

Table 1
Synthesis conditions for graphene-based materials dispersions.

Sample	Immersion time in H_2SO_4(c) (h)	Voltage (V)	Sonication and centrifugation steps	C (mg L^{-1})
Gr-1	0	10	1	71
Gr-2	0	10	3	211
Gr-3	30	10	3	278
Gr-4	30	15	3	370
Gr-5	50	15	3	581
Gr-6	72	15	3	441
Gr-7	50	15	2	410

maximum concentration was considered. In all catalysts, the platinum to be incorporated was added from a 3 mM $H_2PtCl_6.6H_2O$ solution. In the case of the Gr-X/Pt-E catalyst preparation, the mixture was prepared to reach 100 ml of dispersion, while in the Gr-X/Pt–I, Gr-X/Pt–S and Gr-X/Pt–S-R catalysts, it was added to obtain 50 ml dispersion.

2.3. Physicochemical characterization techniques

The morphology of the samples was analyzed by Transmission Electron Microscopy (TEM) using a JEOL (JEM-2010) transmission electron microscope operating at 200 kV with a spatial resolution of 0.24 nm with an EDS detector with INCA Energy TEM platform for chemical analysis of element. Average nanoparticle size and particle size distribution were obtained after measuring ~100 nanoparticles in representative micrographs of each catalyst with the ImageJ software. Field emission scanning electron microscopy (FESEM) has been also used for this purpose using a ZEISS FESEM equipment (Merlin VP Compact) operating at 15 kV with a resolution of 0.8 nm. Pt content was determined by Inductively Coupled Plasma-Optical Emission Spectroscopy (ICP-OES) with a Perkin-Elmer Optima 4300 system. X-ray photoelectron spectroscopy (XPS) analysis was performed in a VG-Microtech Multilab 3000 spectrometer equipped with a semispherical electron analyzer and a Mg Kα ($h\nu = 1253.6$ eV) 300 W X-ray source. Binding energies were referred to the C 1s line at 284.6 eV. Pt 4f, characterized by two well separated spin-orbit coupling components (i.e., Pt $4f_{7/2}$ and Pt $4f_{5/2}$), was analyzed. The deconvolution of the spectra was carried out by using Gaussian functions with 20% of Lorentzian component. FWHM of the peaks was kept between 1.3 and 1.6 eV. A Shirley line was used for estimating the background signal.

The concentration of graphene-based material dispersions was determined by measurement of the weight of the solid residue after evaporation to dryness. These data were correlated with UV–visible spectrophotometry (Jasco V-670 UV–Vis), measuring the absorbance at $\lambda = 270$ nm [49].

Raman spectra were collected using a Jasco NRS-5100 spectrometer employing a 3.9 mW solid-state laser (green) at 532 nm. The spectra were acquired for 120 s. The detector was a Peltier cooled charge-coupled device (CCD) (1024 × 255 pixels). Calibration of the spectrometer was performed with a Si slice (521 ± 2 cm^{-1}). Deconvolution on Lorentzian curves of the G′ band was performed to estimate the number of layers in the graphene-based material dispersions [50,51].

2.4. Electrochemical characterization

The electrochemical characterization was performed in an Autolab PGSTAT302 (Metrohm, Netherlands) potentiostat. A rotating ring-disk electrode (RRDE, Pine Research Instruments, USA) equipped with a glassy carbon disk electrode (5 mm diameter, 0.196 cm^2) and an attached platinum ring, that was used as the working electrodes, graphite as the counter electrode and a reversible hydrogen electrode (RHE) immersed in the working electrolyte through a Luggin capillary as the reference electrode. Electrochemical characterization was performed at 25 °C in a three-electrode cell in 0.1 M KOH and 0.5 M H_2SO_4 media.

Cyclic voltammetry was employed to characterize the samples in both electrolytes in a N_2-saturated atmosphere. For this test, 10 cycles of cyclic voltammetry at 50 mV s^{-1} from 0 V to 1.2 V (vs RHE) were carried out obtaining a steady state voltammogram. The glassy carbon disk was modified with the samples using 120 μL of a 1 mg mL^{-1} dispersion of each electrocatalyts in a water-based solution (20 vol% isopropanol, 0.02 vol% Nafion® in water). Then, the catalyst loading on the glassy carbon electrode was 0.6 mg cm^{-2} in each test.

The ORR was studied by linear sweep voltammetry (LSV) experi-

ments at 5 mVs^{-1} from 1.1 to 0 V (vs RHE), bubbling O_2, in 0.1 M KOH and 0.5 M H_2SO_4 media at 1600 rpm. The Pt ring electrode potential was maintained at 1.5 V during all the measurements. The electron transfer number, n_{e^-}, was calculated from the current used in the hydrogen peroxide oxidation at the Pt ring electrode, according to the following equation [52]:

$$n_{e^-} = \frac{4I_{disk}}{I_{disk} + I_{ring}/N} \quad (1)$$

where I_{disk} and I_{ring} are the currents measured at disk and ring electrodes, respectively, and N is the collection efficiency of the RRDE electrode, which in this case is 0.2534.

In the HER experiment the LSV was conducted at a scan rate of 2 mV s^{-1} from 0.2 V to −0.15 V (vs RHE) bubbling N_2, in 0.1 M KOH at 1600 rpm, and 120 μg of the dispersed material was deposited on the glassy carbon disk.

The amount of Pt deposited on the electrode was different depending on the Pt content of the catalyst measured. Then, to compare the different electrocatalysts, the LSV have been referred to mass of Pt, taking into account the amount of platinum determined by the ICP-OES technique.

The stability for the ORR test was carried out through chronoamperometric experiments with the RRDE at 1600 rpm in O_2-saturated 0.1 M KOH solution at a constant potential of 0.5 V. After 3 h at 0.5 V, methanol was added to the background electrolyte until 1.0 M concentration was reached.

Another ORR stability test was conducted where the most promising graphene-based material was compared to the commercial Pt/C material. For this test 1200 cycles of cyclic voltammetry at 50 mV s^{-1} from a potential of 1.1 V–0 V were carried out. This test was performed in an O_2 saturated 0.1 M KOH electrolyte and the electrode was kept rotating at 1000 rpm.

All electrochemical tests were compared with the commercial material Pt/C (20 wt%).

3. Results and discussion

3.1. Synthesis of graphene-based materials. Optimal synthesis conditions

Table 1 shows the concentration of the dispersions obtained at different conditions. It can be observed that the highest concentration is reached for sample Gr-5. It is known that hydrogen sulphate ions can intercalate within the graphitic layers, generating its expansion and facilitating its subsequent cathodic exfoliation. According to Table 1, the optimum immersion time is 50 h; after that, using 15 V and three sonication and centrifugation steps the highest concentration of the graphene-based material is obtained.

3.2. Graphene-based material characterization

Fig. 2 shows the TEM images of graphene-based material for Gr-4 (Fig. 2a) and Gr-5 (Fig. 2b), which are representative of the observations for these samples. The morphology of the materials corresponds to few-layer graphene material. The dimensions of the layers are between 1 and 10 μm. From EDX analysis of the TEM technique, an oxygen content below 2 wt% and a carbon content higher than 97 wt% are measured, confirming the low oxidation degree of the graphene-based materials obtained with this method.

The structural quality of the graphene-based material was analyzed by Raman spectroscopy. Fig. 3 shows the Raman spectra obtained for Gr-1, Gr-5 and the pristine graphite. As shown in Fig. 3, three bands can be distinguished in the spectra, G band at 1582 cm^{-1}, D band at 1350 cm^{-1} and G′ band at 2700 cm^{-1}. For Gr-1 and Gr-5, G band shifts to wavenumbers higher than 1582 cm^{-1}, which is characteristic of a graphene-based material. Additionally a low intensity of the D band is observed, which is the one produced from stacking defects [53–55].

These results corroborate that the cathodic expansion produces graphene-based materials with low presence of oxygen groups. Fig. 4 shows the deconvolution of the G′ band using Lorentzian curves. Deconvolution for sample Gr-5 using six Lorentzian curves suggests the presence of 3 layers graphene material (Fig. 4a); in the case of sample Gr-1 the deconvolution shows four curves, which can be attributed to 2 layers graphene (Fig. 4b). The higher number of layers in the Gr-5 sample compared to Gr-1 may be due to the higher final concentration of this sample, resulting in a greater agglomeration. However, the material obtained in all samples is still few-layer graphene (less than 5 layers). The deconvolution for pristine graphite in two Lorentzian curves is characteristic for graphite (Fig. 4c) [50,51]. Thus, it can be concluded that the number of predominant layers in the synthesized materials is 2 or 3 layers, which corroborates that our material is a few layers graphene material.

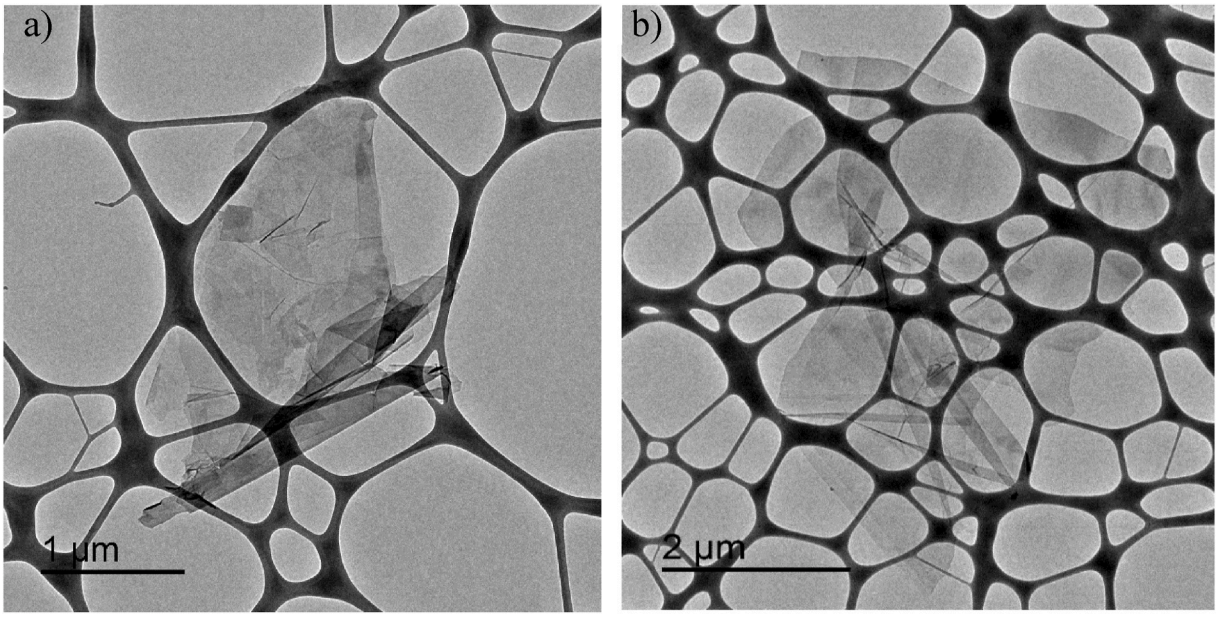

Fig. 2. TEM images **a)** Gr-4 **b)** Gr-5.

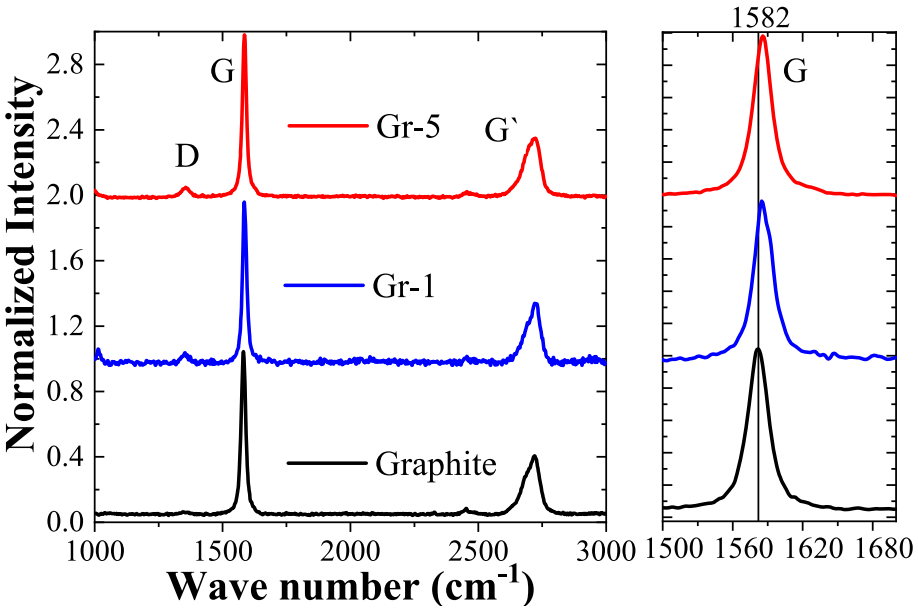

Fig. 3. Raman spectroscopy of graphene-based materials obtained by electrochemical methods.

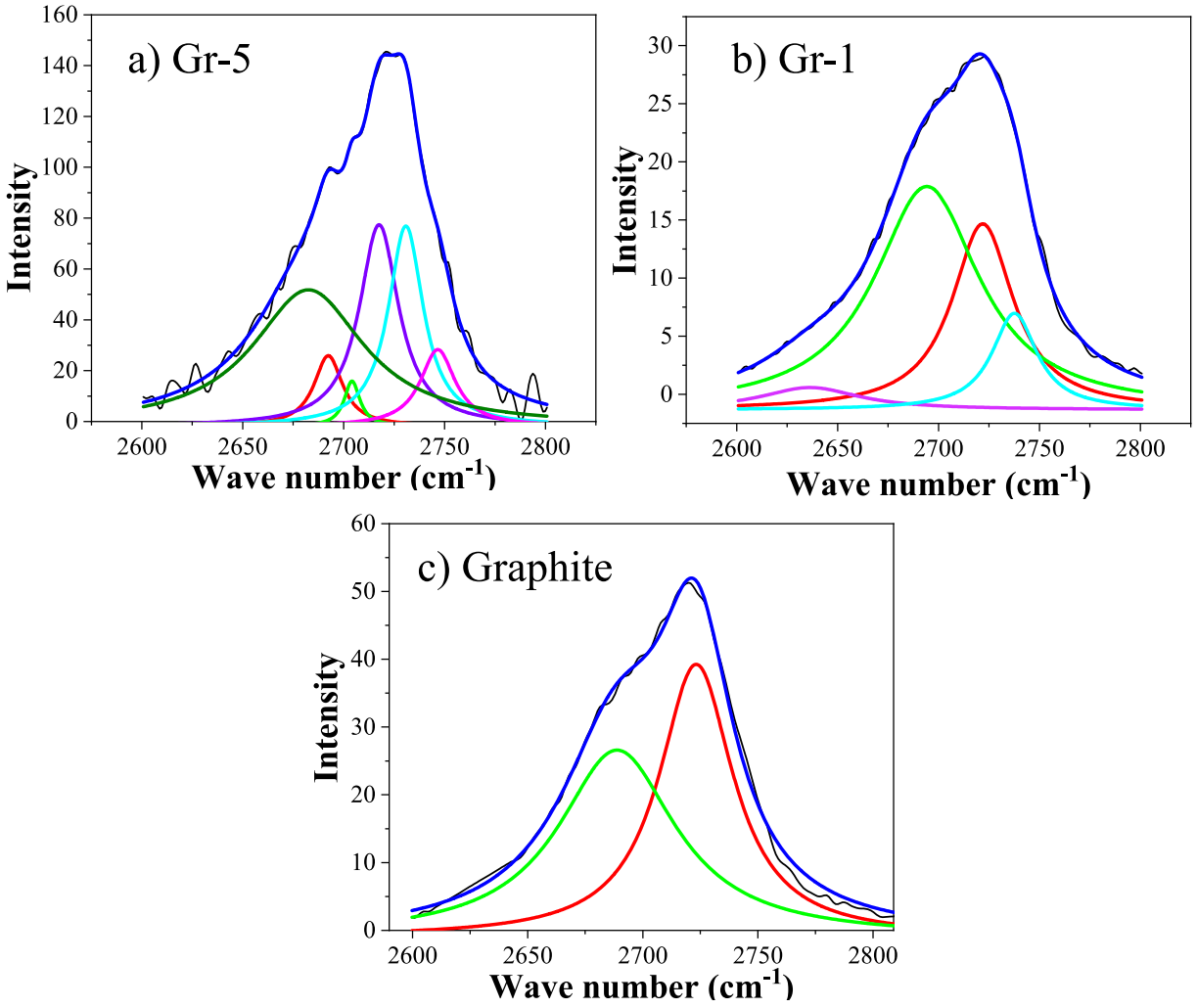

Fig. 4. Deconvolution of G′ band using Lorentzian curves **a)** Gr-5 **b)** Gr-1 **c)** Graphite.

3.3. Pt/graphene-based materials characterization

Figs. S1 and S2 show the micrographs obtained by TEM and FESEM of the graphene-based material obtained after Pt incorporation in the initial immersion step and during the electrochemical expansion step. The incorporation of Pt during the H_2SO_4 immersion step produces a poor distribution of the Pt nanoparticles and the amount of Pt was much lower than the expected 10 wt%, since after the initial stage, washing steps were performed that removed most of the incorporated platinum, leaving only a very low amount in the final graphene-based material (Figs. S1a and S2c and Table 2). The incorporation of Pt during the electrochemical exfoliation step resulted in the sintering of the platinum particles as consequence of the high voltage, generating agglomerates of considerable size, around 100 nm, (Figs. S1b and S2d). In addition, this synthesis procedure generates that the platinum precursor reduces during the electrochemical treatment and the nanoparticles of Pt remains on the graphite sheet avoiding subsequent exfoliation during the sonication step. Then, the amount of Pt incorporated on the graphene-based materials was much higher than 10 wt%, as shown in the XPS and ICP-OES results (Table 2).

Fig. 5 shows the TEM images of Pt/Graphene materials prepared by stirring method and the Pt nanoparticles size distribution. It can be observed that the incorporation of Pt in the graphene-based material dispersions just by stirring and in presence of $NaBH_4$ (Gr-5/Pt–S-R), produced better Pt distribution than the incorporation during the electrochemical exfoliation and during the initial immersion; in this case, Pt nanoparticles of around 5 nm are formed (Fig. 5a and b and S2b). However, the stirring with reducing agent involves a significant number of steps that makes the process time consuming, and additionally, the distribution generated is not still the best, since there are regions of agglomerated nanoparticles. Thus, the method was modified by incorporation of the platinum precursor to the graphene-based material dispersion by stirring for 3 h, with a sonication stage for 1 h and without the addition of reducing agent. In this case (Gr-5/Pt–S), the average particle size obtained was around 1 nm, and the nanoparticle distribution was very good, thus avoiding the agglomeration of nanoparticles (Fig. 5c and d). Fig. S3 shows the Raman spectra obtained for Gr-5/Pt-E, Gr-5/Pt–S, and Gr-5/Pt–S-R. These results show that the presence of platinum does not produce a significant modification of the spectra compared to the pristine graphene-based material (Fig. 3). Thus, it can be concluded that the structure of the graphene-based material remains almost unchanged despite the incorporation of platinum.

Fig. 6 shows the XPS spectra of Pt 4f for the Pt/Graphene-based materials. It is observed that Pt^0 is the main species detected at binding energies of 71.3 and 74.6 eV for Pt $4f_{7/2}$ and $4f_{5/2}$, respectively [54, 56]; a small amount of Pt(II) is also detected being the ratio of both species of 80/20 (Table 2). It must be noted that this ratio is also obtained for Gr-5/Pt–S sample in which no $NaBH_4$ is used for the synthesis. This effect can be attributed to some platinum species reduction by sonolysis that occurs during the ultrasound stage of the synthesis [57]. Fig. S4 shows the XPS spectra of the platinum-containing graphene-based samples obtained with and without sonication to study the effect of the sonication stage in the reduction of the platinum species. The sample prepared without the sonication stage in the platinum incorporation will be referred to as Gr-5/Pt-S-NS. As we can observe, the sonication step produces a greater reduction of the platinum species and in the sample Gr-5/Pt-S-NS only a partial reduction of Pt^{+4} to Pt^{+2} species occurs. However, the partial reduction of platinum in the sample without the sonication step suggests the contribution of the graphene material in the reduction process, in agreement with previous studies that have demonstrated the effect of the carbon material in the spontaneous reduction of metal ions [58–60]. Then, it can be concluded that the carbon material itself facilitates the reduction of the Pt precursor.

To confirm the amount of platinum loaded, ICP-OES was performed. Table 2 shows the summary of characterization of the different Pt/Graphene-based catalyst by XPS and ICP-OES. The results showed that a 10 wt% of Pt was incorporated for Gr-5/Pt–S. The incorporation by stirring was studied and the addition to the dispersion of 11 wt% of Pt resulted in the incorporation of the desired 10 wt%, obtaining a loading efficiency of 91%. For the other samples, the amount of platinum incorporated was not the desired; in the case of Gr-5/Pt–I it was less than 0.5 wt%, for Gr-5/Pt-E the incorporation exceeded 60 wt%, and for Gr-5/Pt–S-R it was approximately 27 wt%. The higher amount of Pt obtained in this catalyst is attributed to the subsequent stages applied in the $NaBH_4$ addition process, which included a centrifugation step, that eliminates graphene material and increases the platinum ratio. These results show the difficulty in controlling the amount of platinum and that the incorporation of Pt in these steps is not adequate. However, the simple incorporation of the Pt precursor in the colloidal graphene-based material, without the addition of $NaBH_4$, results in an efficient incorporation of Pt nanoparticles with the desired amount, showing that the graphene-based material acts as support for Pt nanoparticles and, on the other hand, as an efficient physical barrier to prevent platinum nanoparticle aggregation. Probably, graphene layers can cover the Pt nanoparticles preventing the agglomeration. Then, graphene layers could inhibit nanoparticle aggregation by self-assembling onto graphene nanosheets and forming a two-dimensional (2D) layered nanocomposite [61].

Table 2
Pt content in Pt/Graphene-based catalysts by XPS and ICP-OES.

Catalyst	Pt (wt%) (XPS)	%Pt(0) (XPS)	% Pt(II) (XPS)	Pt (wt%) (ICP-OES)
Gr-5/Pt–I	0.8	71.4	28.6	0.29
Gr-5/Pt-E	64.8	72.2	27.8	60.3
Gr-5/Pt–S	12.9	82.1	17.9	10.6
Gr-5/Pt–S-R	20.5	78.8	21.2	27.0
Pt/C	21.8	70.4	29.6	21.5

3.4. Electrochemical characterization

Figs. S5 and S6 shows the voltammograms for different electrocatalysts in alkaline and acid medium, respectively. It can be seen that the characteristic voltametric profile of Pt is clearly observed for Gr-5/Pt–S and the commercial Pt/C catalysts, which confirms the correct incorporation of Pt on the surface of the carbon materials. In the case of the Gr-5/Pt–S-R, these processes are less pronounced, possibly due to a poorer distribution of the Pt nanoparticles on the surface of the graphene material. The electrical charge integrated under the so-called hydrogen desorption peak in the potential range between 0.05 and 0.4 V can be used (after double layer correction) to determine the electrochemical surface area (ECSA) of Pt considering 210 μC cm^{-2} as the reference value for the adsorption of one-electron process per surface Pt atom. Table 3 includes the values of ECSA for the Pt supported on the graphene-based materials and the commercial catalyst (expressed per gram of Pt). It can be observed that the electrochemical surface area value for the Gr-5/Pt–S catalyst is similar to the Pt/C commercial electrocatalyst, whereas the value for Gr-5/Pt–S-R material is much lower, what is in agreement with the TEM observations.

3.4.1. Electrochemical activity towards oxygen reduction reaction (ORR)

The electrochemical activity of the different electrocatalysts was evaluated employing a RRDE in 0.1 M KOH and 0.5 M H_2SO_4 solutions. Fig. 7 shows the results for the graphene-based electrocatalysts in alkaline and acid media. Fig. 7a shows the LSV curves for alkaline medium in which the material with the highest electrocatalytic activity is the one obtained by incorporating Pt during stirring and without reducing agent (Gr-5/Pt–S). The onset potential for this electrocatalyst measured at −0.1 mA cm^{-2} and the half-wave potential are very close to that of the commercial Pt/C catalyst (Table 3), and it also achieves a limiting current density like the commercial one but using only half of

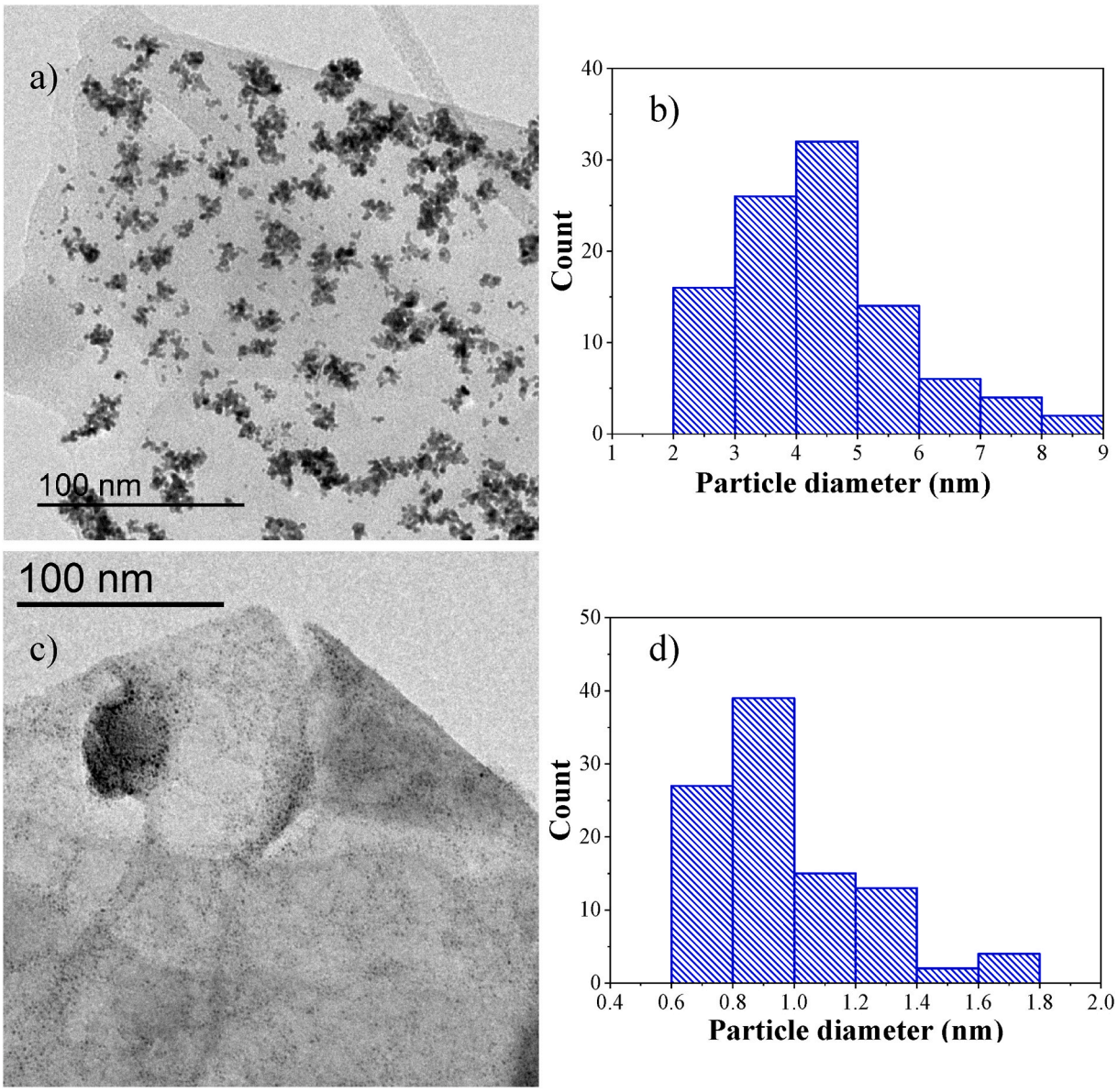

Fig. 5. TEM images of Pt nanoparticles supported on graphene-based material by stirring method a) with $NaBH_4$ (Gr-5/Pt–S-R) c) without $NaBH_4$ (Gr-5/Pt–S) and histogram of particle size distribution of Pt b) Gr-5/Pt–S-R and d) Gr-5/Pt–S samples.

weight of platinum. The reason why Gr-5/Pt–S catalyst is much more active despite having a lower metal content than the commercial material is attributed to a synergistic effect between the graphene-based material and the Pt that generates an excellent distribution of the Pt nanoparticles with a particle size of around 1 nm. The catalytic activity for this sample is much higher than for Gr-5/Pt–S-R sample, that has a much higher platinum content, what is in agreement with the larger the particle size and worse distribution of Pt nanoparticles in this catalyst. In addition, the carbon material support is a few-layer graphene material with a low degree of oxidation which favors a high electrical conductivity.

It is also worth noting the clear tendency of the different electrocatalysts to follow the 4-electron pathway (Fig. 7b), which is the most energetically efficient and the desired pathway in this reaction.

To analyze the effect of sonication in ORR activity, the sample without $NaBH_4$ reduction and without sonication treatment has been studied (Gr-5/Pt-S-NS). The LSV curve for Gr-5/Pt-S-NS catalyst has been added in Fig. 7a and b. As can be observed, this sample shows a significant decrease in catalytic activity in comparison to Gr-5/Pt–S sample, with a worse onset potential, limiting current and number of electrons transferred. This indicates that the sonication step is necessary to obtain a good electrocatalyst probably as consequence of the larger amount of reduced platinum and the better distribution achieved in the platinum nanoparticles.

Fig. 7c also shows a very good performance for Gr-5/Pt–S for ORR in acid medium, showing an onset potential, a limiting current density close to the commercial Pt/C material and a high selectivity to the 4-electron pathway (Table 3). The ring current obtained from the LSV in Fig. 7 is represented in Fig. S7.

Fig. 8 shows the LSV for the electrocatalysts studied in the ORR comparing the mass-specific activity, taking into account the amount of platinum in each electrocatalyst as determined by the ICP-OES technique.

From these results, it can be concluded that the graphene-based material with Pt nanoparticles incorporated by stirring (Gr-5/Pt–S) and without using reducing agent shows a good electrocatalytic performance, which makes it a promising alternative to the Pt/C commercial material for the ORR in alkaline and acid media. It must be

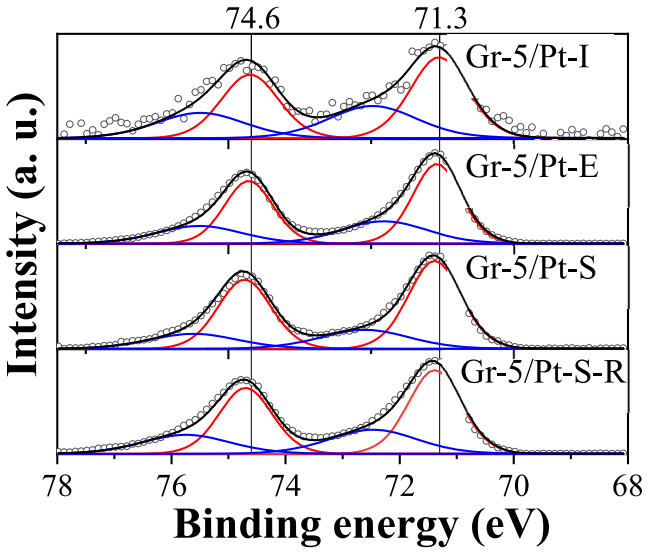

Fig. 6. XPS spectra of Pt 4f for the different electrocatalysts.

emphasized that the synthesis does not use any protecting agent to achieve a low Pt particle size, and that the graphene-based material itself acts as reducing agent and prevents Pt nanoparticle from sintering.

The Tafel slopes of all catalysts listed in Table 3 were determined from Tafel plots (see Figs. S8a and b). It can be observed that Tafel slopes for all platinum-based electrocatalysts in alkaline and acid medium are close to that of the commercial Pt/C sample (61 mV dec^{-1} and 82 mV dec^{-1}, respectively), which indicates that the ORR kinetics are similar for all Pt-based electrocatalysts.

The stability of the most promising sample was tested by a chronoamperometric technique, and the results are shown in Fig. 9. The experiment was performed in an RRDE at 1600 rpm in O_2-saturated 0.1 M KOH electrolyte and at a constant potential of 0.5 V, where the limited current is reached [62]. The commercial Pt/C sample was tested under the same experimental conditions to compare the stability of the synthesized material. After about 3 h at 0.5 V, methanol was added to the working electrolyte until a concentration of 1.0 M was reached. As expected, the Pt-based catalyst maintains almost 95% of the initial current after around 170 min. However, after the addition of methanol to the working electrolyte, the current suddenly drops to zero because the active metal is poisoned by CO from the decomposition/oxidation of methanol. The activity of the graphene-based material Gr-5/Pt–S shows a slow decay that tends to stabilize at around 120–170 min. After the addition of methanol, the graphene-based catalyst shows a high tolerance to poisoning, what is quite remarkable since the active phase of the material is Pt; nevertheless, it seems that thanks to the graphene acting as a protective agent for CO poisoning, probably because the graphene layers cover the platinum surface and facilitates the electron transfer [63], total poisoning is avoided and only a small current drop of about 9% is recorded at the end of the experiment. From the results of this test, it can be concluded that the graphene-based material shows good electrocatalytic performance which makes it a promising alternative and shows excellent behavior against CO poisoning.

The results for the second durability test are shown in Fig. S9, the voltammograms obtained after the 1200 cycles of cyclic voltammetry at 50 mV s^{-1} from a potential of 0 V–1.1 V in O_2 saturated atmosphere by bubbling and the electrode was kept rotating at 1000 rpm; this test was performed in 0.1 M KOH. As can be seen in both catalysts there is a significant decrease in the intensity, although the commercial material retains the voltametric profile of a Pt electrode, while in the graphene-based material, these voltametric profiles are no longer appreciated.

3.4.2. *Electrochemical activity towards hydrogen evolution reaction (HER)*

Fig. 10 shows that sample Gr-5/Pt–S has a very good performance for HER. In this experiment, the LSV was conducted at a scan rate of 2 mV s^{-1} from 0.2 V to −0.15 V (vs RHE), to prevent the production of hydrogen in large quantities and avoid the material dropping; this experiment was carried out in 0.1 M KOH. Excellent results were obtained, in which a current of 9.7 mA cm^{-2} is reached at −0.15 V versus 6.9 mA cm^{-2} for the Pt/C-Commercial material, showing a superior performance but using only half of weight of platinum. In addition, the reaction onset potential shows a value close to 0 V, which is the optimal for the electrocatalysts of HER.

To compare the stability of the samples against the HER, a cyclic voltammetry test of 500 cycles with a scan rate of 100 mV s^{-1}, in a range of potentials between 0.1 and −0.1 V, a region where the hydrogen production occurs for these materials [64], was performed in rotation at 1600 rpm to eliminate the H_2 bubbles produced and was done in 0.1 M KOH saturated with N_2. After cycling, LSV was measured and compared to the initial LSV. Fig. S10 shows the first and last voltammograms for the Gr-5/Pt–S catalyst. As can be seen, there is a small decrease in activity with the cycles; however, after the test the catalyst is still very active towards this reaction. As shown in Fig. 11, Gr-5/Pt–S and Pt/C-Commercial materials show a decrease in activity; however, it is noteworthy that the Pt/graphene-based still has higher current than the commercial material (9.33 mA cm^{-2} is reached at −0.15 V versus 6.5 mA cm^{-2} for the Pt/C-Commercial material), and the decrease in activity for this catalyst compared to the initial test is 3.8% whereas that of the commercial material is 5.8%. Thus, it can be concluded the excellent performance of the Gr-5/Pt–S synthesized sample towards the HER, outperforming the Pt/C commercial material despite using half of the metal loading. The results support the critical role of the Pt nanoparticles distribution and size in the catalysis of hydrogen evolution.

Table 3
Electrochemical parameters obtained from LSV curves to the ORR in alkaline and acid medium. The limit current density and the electron transfer number have been determined at 0.4 V.

Alkaline medium							
Catalyst	E (Onset) (V) (at −0.1 mA cm^{-2})	j (mA cm^{-2}) (at 0.4V)	j (A g_{Pt}^{-1}) (at 0.4V)	n_e (0.4V)	ECSA (m^2 g^{-1}Pt)	Half-wave potential (V)	Tafel slope (mV dec^{-1})
Gr-5	0.70	1.5	–	2.5	–	0.59	109
Gr-5/Pt–S	0.98	5.7	94	4	30	0.81	61
Gr-5/Pt–S-R	0.88	4.0	20	3.7	5	0.73	60
Pt/C	0.99	5.7	51	4	37	0.87	61
Acid Medium							
Gr-5	–	0.2	–	3.1	–	0.27	–
Gr-5/Pt–S	0.96	4.5	73	4	32	0.78	75
Gr-5/Pt–S-R	0.93	3.2	17	3.9	12	0.76	76
Pt/C	0.98	5	40	4	36	0.85	82

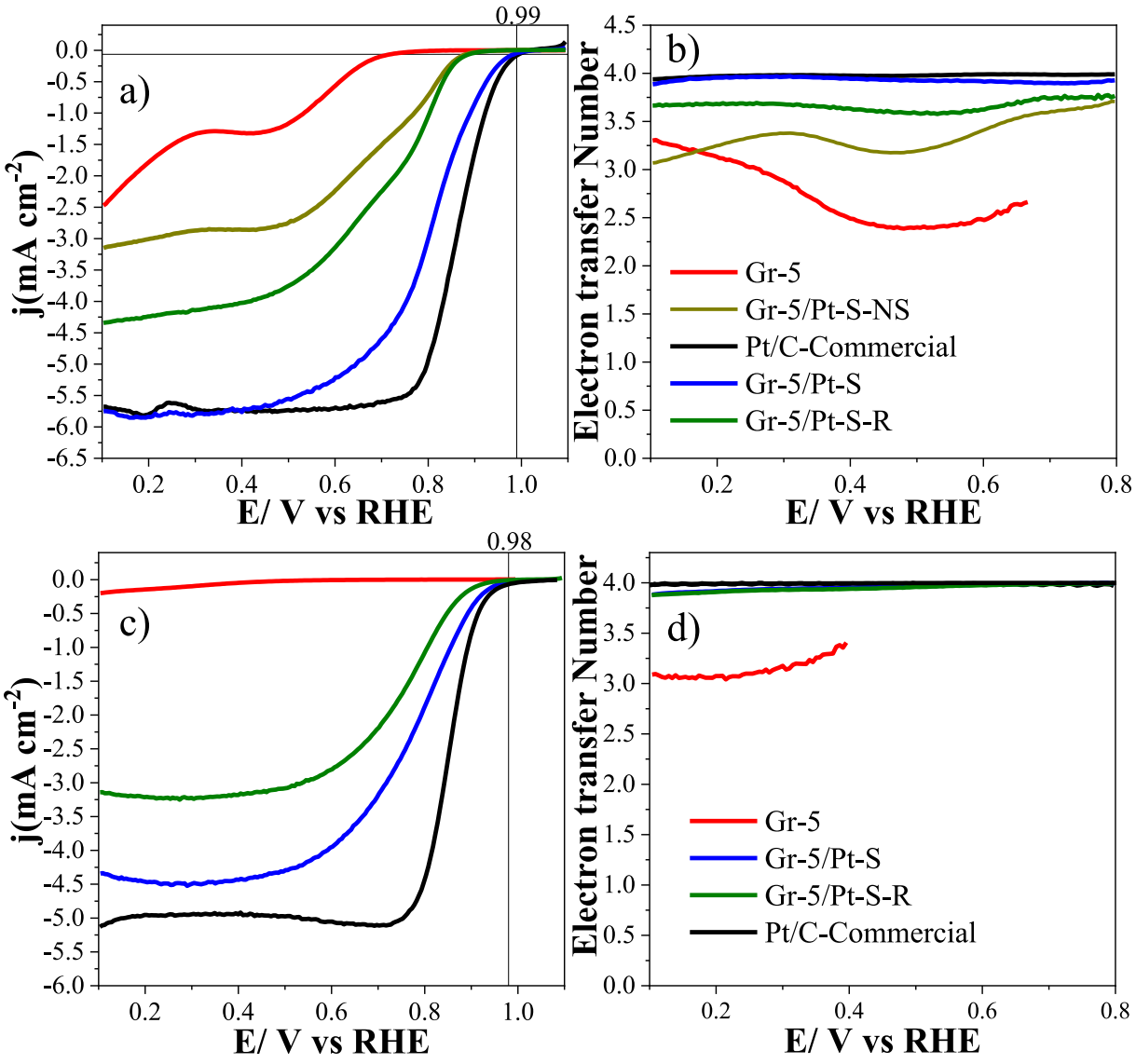

Fig. 7. Linear sweep voltammograms obtained with the rotating disc electrode for the graphene-based samples in **a)** 0.1 M KOH, **c)** 0.5 M H_2SO_4. Saturated with O_2 at 1600 rpm. V = 5 mV s^{-1}. Electron transfer number in **b)** 0.1 M KOH, **d)** 0.5 M H_2SO_4.

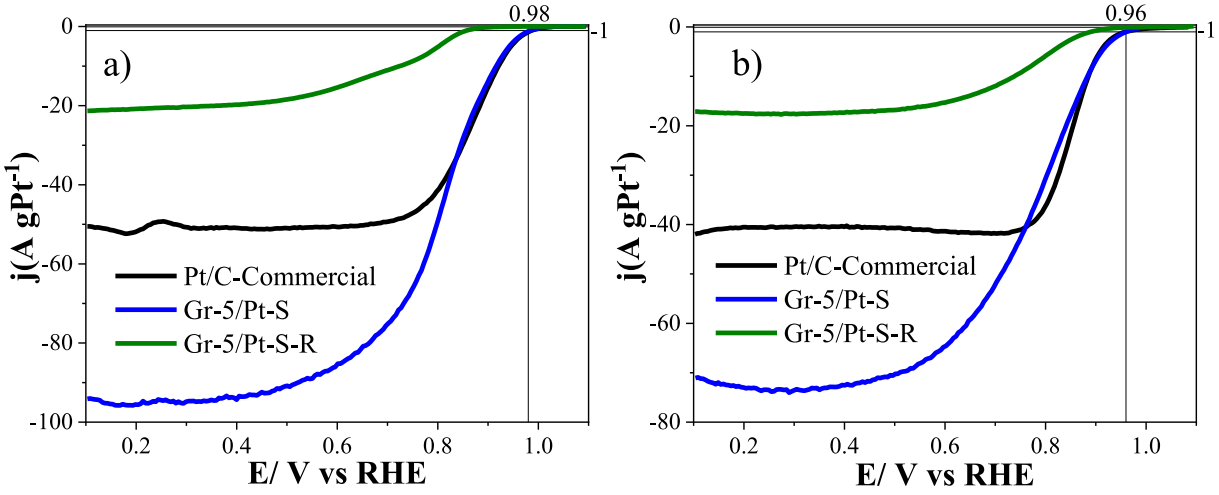

Fig. 8. LSV referred to mass-specific activity of the different electrocatalysts obtained in **a)** 0.1 M KOH, **b)** 0.5 M H_2SO_4. saturated with O_2 at 1600 rpm. V = 5 mV s^{-1}.

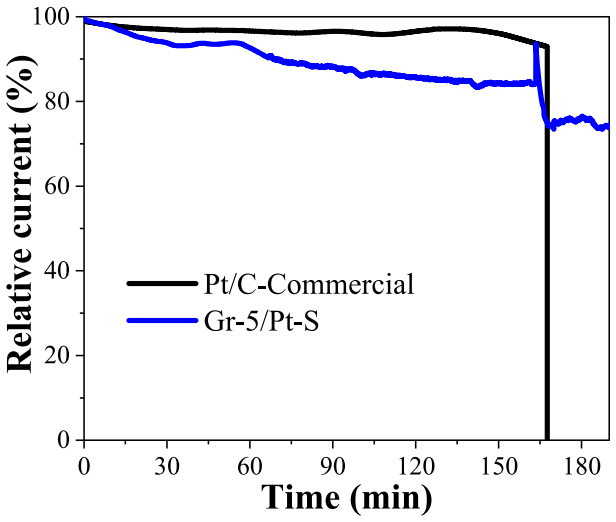

Fig. 9. Comparative stability test for Gr-5/Pt–S and Pt/C-commercial accomplished at 0.5 V and 1600 rpm in O_2-saturated 0.1 M KOH and 25 °C. Methanol was added 170 min after the beginning of the experiment.

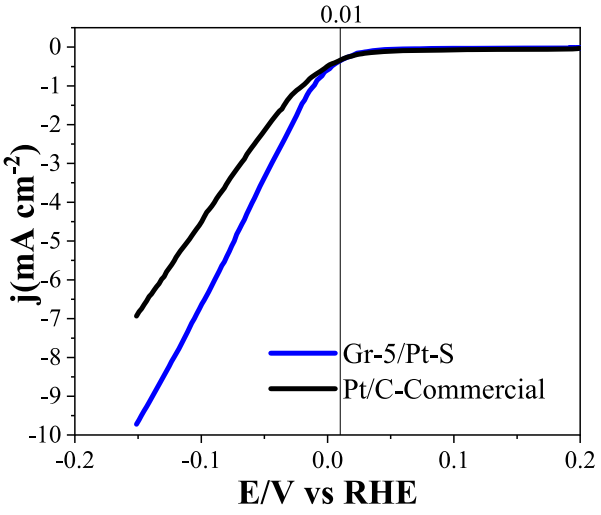

Fig. 10. Linear sweep voltammograms for Gr-5/Pt–S and Pt/C-Commercial for HER, in 0.1 M KOH saturated with N_2. Scan rate of 2 mV s^{-1} from 0.2 V to −0.15 V (vs RHE).

4. Conclusions

Graphene-based materials were synthesized by electrochemical exfoliation method (cathodic expansion), obtaining few layer graphene dispersions with a low oxidation degree with an oxygen content of less than 2%. The optimal experimental conditions were established to obtain the highest concentration of few layers graphene material without altering the properties of the graphene-based materials, being these conditions 50 h in the initial immersion in concentrated sulfuric acid, 15 V in the cathodic expansion stage, and 3 times of sonication and centrifugation step. For the synthesis of the Pt electrocatalysts for ORR and HER, the study of the incorporation of platinum was done in each of the steps of the graphene-based material synthesis. The incorporation of platinum in the graphene-based material dispersion with stirring for 3 h and sonication for 1 h, without using any reducing and protecting agents to avoid sintering of nanoparticles, produced a 10 wt% Pt catalyst with an average particle size of about 1 nm and with an excellent distribution on the graphene-based material support. The easiness of the synthesis is determined by the presence of the graphene-based material that acts as

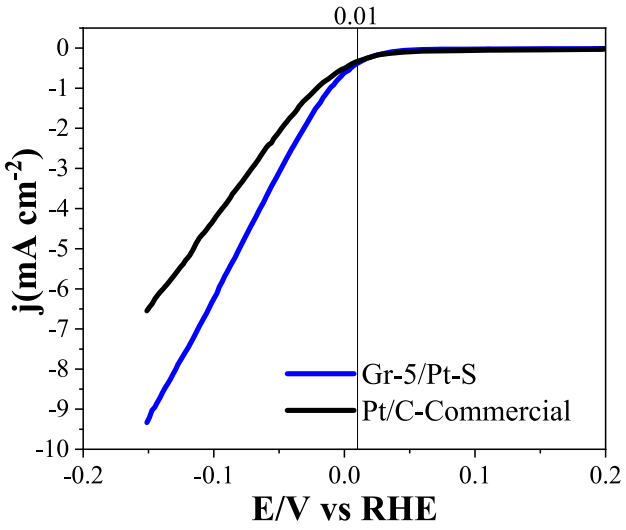

Fig. 11. Linear sweep voltammograms after the 500 cycles for Gr-5/Pt–S and Pt/C-Commercial for HER, in 0.1 M KOH saturated with N_2. Scan rate of 2 mV s^{-1} from 0.2 V to −0.15 V (vs RHE).

both reducing and protecting agent against platinum nanoparticle sintering.

Finally, this electrocatalyst has an excellent behavior in both acid and alkaline medium, with high onset potential (0.98 vs 0.99 V in alkaline medium), high half-wave potential (0.81 vs 0.87 V in alkaline medium) and excellent current density for both ORR and HER, which has a similar performance to the commercial Pt/C material that contains a 20 wt% of Pt and when compared in mass-specific activity significantly outperforms it. Furthermore, it is noteworthy that the catalysts presents high methanol resistance to CO poisoning, what can be attributed to the protective action of the graphene layers that may cover the Pt surface avoiding poisoning.

CRediT author statement

Authors contributed equally to this work.

Declaration of competing interest

The authors declare that they have no known competing financial interests or personal relationships that could have appeared to influence the work reported in this paper.

Data availability

Data will be made available on request.

Acknowledgements

The authors would like to thank PID2019-105923RB-I00 and PID2021-123079OB-I00 projects funded by MCIN/AEI/10.13039/501100011033 and “ERDF A way of making Europe”, and the Generalitat Valenciana (GRISOLIA/2020/114) for the financial support.

Appendix A. Supplementary data

Supplementary data to this article can be found online at https://doi.org/10.1016/j.energy.2023.127888.

References

[1] Nasir S, Hussein MZ, Zainal Z, Yusof NA. Carbon-based nanomaterials/allotropes: a glimpse of their synthesis, properties and some applications. Materials 2018;11:1–24. https://doi.org/10.3390/ma11020295.

[2] Fan X, Chen X, Dai L. 3D graphene based materials for energy storage. Curr Opin Colloid Interface Sci 2015;20:429–38. https://doi.org/10.1016/j.cocis.2015.11.005.

[3] Dai L, Chang DW, Baek JB, Lu W. Carbon nanomaterials for advanced energy conversion and storage. Small 2012;8:1130–66. https://doi.org/10.1002/smll.201101594.

[4] Nazir H, Louis C, Jose S, Prakash J, Muthuswamy N, Buan MEM, et al. Is the H2 economy realizable in the foreseeable future? Part I: H_2 production methods. Int J Hydrogen Energy 2020;45:13777–88. https://doi.org/10.1016/j.ijhydene.2020.03.092.

[5] Nazir H, Muthuswamy N, Louis C, Jose S, Prakash J, Buan ME, et al. Is the H2 economy realizable in the foreseeable future? Part II: H_2 storage, transportation, and distribution. Int J Hydrogen Energy 2020;45:20693–708. https://doi.org/10.1016/j.ijhydene.2020.05.241.

[6] Nazir H, Muthuswamy N, Louis C, Jose S, Prakash J, Buan MEM, et al. Is the H2 economy realizable in the foreseeable future? Part III: H_2 usage technologies, applications, and challenges and opportunities. Int J Hydrogen Energy 2020;45:28217–39. https://doi.org/10.1016/j.ijhydene.2020.07.256.

[7] Ray SC. Application and uses of graphene. In: Appl. Graphene graphene-oxide based nanomater. Elsevier; 2015. p. 1–38. https://doi.org/10.1016/B978-0-323-37521-4.00001-7.

[8] Novoselov KS, Fal'Ko VI, Colombo L, Gellert PR, Schwab MG, Kim K. A roadmap for graphene. Nature 2012;490:192–200. https://doi.org/10.1038/nature11458.

[9] Morozov SV, Novoselov KS, Katsnelson MI, Schedin F, Elias DC, Jaszczak JA, et al. Giant intrinsic carrier mobilities in graphene and its bilayer. Phys Rev Lett 2008;100:11–4. https://doi.org/10.1103/PhysRevLett.100.016602.

[10] Mayorov AS, Gorbachev RV, Morozov SV, Britnell L, Jalil R, Ponomarenko LA, et al. Micrometer-scale ballistic transport in encapsulated graphene at room temperature. Nano Lett 2011;11:2396–9. https://doi.org/10.1021/nl200758b.

[11] Lee C, Wei X, Kysar JW, Hone J. Measurement of the elastic properties and intrinsic strength of monolayer graphene. Science 2008;321:385–8. https://doi.org/10.1126/science.1157996.

[12] Liu F, Ming P, Li J. Ab initio calculation of ideal strength and phonon instability of graphene under tension. Phys Rev B Condens Matter 2007;76:1–7. https://doi.org/10.1103/PhysRevB.76.064120.

[13] Novoselov KS, Geim AK, V Morozov S, Jiang D, Zhang Y, Dubonos SV, et al. Electric field effect in atomically thin carbon films supplementary. Science 2004;5:1–12. https://doi.org/10.1126/science.aab1343. 80-.

[14] Dean CR, Young AF, Meric I, Lee C, Wang L, Sorgenfrei S, et al. Boron nitride substrates for high-quality graphene electronics. Nat Nanotechnol 2010;5:722–6. https://doi.org/10.1038/nnano.2010.172.

[15] Najafabadi AT, Gyenge E. Synergistic production of graphene microsheets by simultaneous anodic and cathodic electro-exfoliation of graphitic electrodes in aprotic ionic liquids. Carbon 2015;84:449–59. https://doi.org/10.1016/j.carbon.2014.12.041.

[16] Marcano DC, Kosynkin DV, Berlin JM, Sinitskii A, Sun Z, Slesarev A, et al. Improved synthesis of graphene oxide. ACS Nano 2010;4:4806–14. https://doi.org/10.1021/nn1006368.

[17] Wypych G. Production of graphene and its derivatives. In: Graphene important results and applications. Elsevier; 2019. p. 9–84. https://doi.org/10.1016/b978-1-927885-51-2.50005-5.

[18] Berger C, Song Z, Li X, Wu X, Brown N, Naud C, et al. Electronic confinement and coherence in patterned epitaxial graphene. Science 2006;312:1191–6. https://doi.org/10.1126/science.1125925. 80-.

[19] Kim KS, Zhao Y, Jang H, Lee SY, Kim JM, Kim KS, et al. Large-scale pattern growth of graphene films for stretchable transparent electrodes. Nature 2009;457:706–10. https://doi.org/10.1038/nature07719.

[20] Li X, Cai W, An J, Kim S, Nah J, Yang D, et al. Large-area synthesis of high-quality and uniform graphene films on copper foils. Science 2009;324:1312–4. https://doi.org/10.1126/science.1171245. 80-.

[21] Low CTJ, Walsh FC, Chakrabarti MH, Hashim MA, Hussain MA. Electrochemical approaches to the production of graphene flakes and their potential applications. Carbon 2013;54:1–21. https://doi.org/10.1016/j.carbon.2012.11.030.

[22] Aghamohammadi H, Eslami-Farsani R, Torabian M, Amousa N. Recent advances in one-pot functionalization of graphene using electrochemical exfoliation of graphite: a review study. Synth Met 2020;269:116549. https://doi.org/10.1016/j.synthmet.2020.116549.

[23] Ji Z, Perez-Page M, Chen J, Rodriguez RG, Cai R, Haigh SJ, et al. A structured catalyst support combining electrochemically exfoliated graphene oxide and carbon black for enhanced performance and durability in low-temperature hydrogen fuel cells. Energy 2021;226:120318. https://doi.org/10.1016/j.energy.2021.120318.

[24] Yang S, Lohe MR, Müllen K, Feng X. New-generation graphene from electrochemical approaches: production and applications. Adv Mater 2016;28:6213–21. https://doi.org/10.1002/adma.201505326.

[25] Abdelkader AM, Cooper AJ, Dryfe RAW, Kinloch IA. How to get between the sheets: a review of recent works on the electrochemical exfoliation of graphene materials from bulk graphite. Nanoscale 2015;7:6944–56. https://doi.org/10.1039/c4nr06942k.

[26] García-Dalí S, Paredes JI, Munuera JM, Villar-Rodil S, Martínez-Alonso A, Tascón JMD. An aqueous cathodic delamination route towards high quality graphene flakes for oil sorption and electrochemical charge storage applications. Chem Eng J 2019;372:1226–39. https://doi.org/10.1016/j.cej.2019.04.201.

[27] Zhang Y, Xu Y, Liu R. Regulating cations and solvents of the electrolyte for ultra-efficient electrochemical production of high-quality graphene. Carbon 2021;176:157–67. https://doi.org/10.1016/j.carbon.2021.01.109.

[28] Li F, Xue M, Zhang X, Chen L, Knowles GP, MacFarlane DR, et al. Advanced composite 2D energy materials by simultaneous anodic and cathodic exfoliation. Adv Energy Mater 2018;8:1–8. https://doi.org/10.1002/aenm.201702794.

[29] Alanyalioğlu M, Segura JJ, Oró-Sol J, Casañ-Pastor N. The synthesis of graphene sheets with controlled thickness and order using surfactant-assisted electrochemical processes. Carbon 2012;50:142–52. https://doi.org/10.1016/j.carbon.2011.07.064.

[30] Wang J, Manga KK, Bao Q, Loh KP. High-yield synthesis of few-layer graphene flakes through electrochemical expansion of graphite in propylene carbonate electrolyte. J Am Chem Soc 2011;133:8888–91. https://doi.org/10.1021/ja203725d.

[31] Debe MK. Electrocatalyst approaches and challenges for automotive fuel cells. Nature 2012;486:43–51. https://doi.org/10.1038/nature11115.

[32] Gómez-Marín A, Feliu J, Edson T. Reaction mechanism for oxygen reduction on platinum: existence of a fast initial chemical step and a soluble species different from H_2O_2. ACS Catal 2018;8:7931–43. https://doi.org/10.1021/acscatal.8b01291.

[33] Shao M, Chang Q, Dodelet JP, Chenitz R. Recent advances in electrocatalysts for oxygen reduction reaction. Chem Rev 2016;116:3594–657. https://doi.org/10.1021/acs.chemrev.5b00462.

[34] Hussain S, Erikson H, Kongi N, Sarapuu A, Solla-Gullón J, Maia G, et al. Oxygen reduction reaction on nanostructured Pt-based electrocatalysts: a review. Int J Hydrogen Energy 2020;45:31775–97. https://doi.org/10.1016/j.ijhydene.2020.08.215.

[35] Eftekhari A. Electrocatalysts for hydrogen evolution reaction. Int J Hydrogen Energy 2017;42:11053–77. https://doi.org/10.1016/j.ijhydene.2017.02.125.

[36] Ojani R, Valiollahi R, Raoof J-B. Comparison between graphene supported Pt hollow nanospheres and graphene supported Pt solid nanoparticles for hydrogen evolution reaction. Energy 2014;74:871–6. https://doi.org/10.1016/j.energy.2014.07.062.

[37] Lasia A. Hydrogen evolution reaction. In: Handb. Fuel cells. Chichester, UK: John Wiley & Sons, Ltd; 2010. https://doi.org/10.1002/9780470974001.f204033.

[38] Jaramillo TF, Jørgensen KP, Bonde J, Nielsen JH, Horch S, Chorkendorff I. Identification of active edge sites for electrochemical H_2 evolution from MoS_2 nanocatalysts. Science 2007:100–2. https://doi.org/10.1126/science.1141483. 80-.). 317.

[39] Voiry D, Yamaguchi H, Li J, Silva R, Alves DCB, Fujita T, et al. Enhanced catalytic activity in strained chemically exfoliated WS_2 nanosheets for hydrogen evolution. Nat Mater 2013;12:850–5. https://doi.org/10.1038/nmat3700.

[40] Antolini E. Graphene as a new carbon support for low-temperature fuel cell catalysts. Appl Catal B Environ 2012:52–68. https://doi.org/10.1016/j.apcatb.2012.04.022. 123–124.

[41] Duan J, Chen S, Chambers BA, Andersson GG, Qiao SZ. 3D WS2 Nanolayers@Heteroatom-doped graphene films as hydrogen evolution catalyst electrodes. Adv Mater 2015;27:4234–41. https://doi.org/10.1002/adma.201501692.

[42] Qu L, Liu Y, Baek JB, Dai L. Nitrogen-doped graphene as efficient metal-free electrocatalyst for oxygen reduction in fuel cells. ACS Nano 2010;4:1321–6. https://doi.org/10.1021/nn901850u.

[43] Sheng ZH, Gao HL, Bao WJ, Bin Wang F, Xia XH. Synthesis of boron doped graphene for oxygen reduction reaction in fuel cells. J Mater Chem 2012;22:390–5. https://doi.org/10.1039/c1jm14694g.

[44] Liang Y, Li Y, Wang H, Zhou J, Wang J, Regier T, et al. Co_3O_4 nanocrystals on graphene as a synergistic catalyst for oxygen reduction reaction. Nat Mater 2011;10:780–6. https://doi.org/10.1038/nmat3087.

[45] Wang L, Dong H, Guo Z, Zhang L, Hou T, Li Y. Potential application of novel boron-doped graphene nanoribbon as oxygen reduction reaction catalyst. J Phys Chem C 2016;120:17427–34. https://doi.org/10.1021/acs.jpcc.6b04639.

[46] Chou C-C, Liu C-H, Chen B-H. Effects of reduction temperature and pH value of polyol process on reduced graphene oxide supported Pt electrocatalysts for oxygen reduction reaction. Energy 2014;70:231–8. https://doi.org/10.1016/j.energy.2014.03.118.

[47] Beltrán-Gastélum M, Salazar-Gastélum MI, Flores-Hernández JR, Botte GG, Pérez-Sicairos S, Romero-Castañon T, et al. Pt-Au nanoparticles on graphene for oxygen reduction reaction: stability and performance on proton exchange membrane fuel cell. Energy 2019;181:1225–34. https://doi.org/10.1016/j.energy.2019.06.033.

[48] Ensafi AA, Nabiyan A, Jafari-Asl M, Dinari M, Farrokhpour H, Rezaei B. Galvanic exchange at layered doubled hydroxide/N-doped graphene as an in-situ method to fabricate powerful electrocatalysts for hydrogen evolution reaction. Energy 2016;116:1087–96. https://doi.org/10.1016/j.energy.2016.10.048.

[49] Munuera JM, Paredes JI, Villar-Rodil S, Martínez-Alonso A, Tascón JMD. A simple strategy to improve the yield of graphene nanosheets in the anodic exfoliation of graphite foil. Carbon 2017;115:625–8. https://doi.org/10.1016/j.carbon.2017.01.038.

[50] Malard LM, Pimenta MA, Dresselhaus G, Dresselhaus MS. Raman spectroscopy in graphene. Phys Rep 2009;473:51–87. https://doi.org/10.1016/j.physrep.2009.02.003.

[51] Graf D, Molitor F, Ensslin K, Stampfer C, Jungen A, Hierold C, et al. Spatially resolved Raman spectroscopy of single- and few-layer graphene. Nano Lett 2007;7:238–42. https://doi.org/10.1021/nl061702a.

[52] Zhou R, Zheng Y, Jaroniec M, Qiao SZ. Determination of the electron transfer number for the oxygen reduction reaction: from theory to experiment. ACS Catal 2016;6:4720–8. https://doi.org/10.1021/acscatal.6b01581.
[53] Ferrari AC, Basko DM. Raman spectroscopy as a versatile tool for studying the properties of graphene. Nat Nanotechnol 2013;8:235–46. https://doi.org/10.1038/nnano.2013.46.
[54] Munuera JM, Paredes JI, Villar-Rodil S, Ayán-Varela M, Martínez-Alonso A, Tascón JMD. Electrolytic exfoliation of graphite in water with multifunctional electrolytes: en route towards high quality, oxide-free graphene flakes. Nanoscale 2016;8:2982–98. https://doi.org/10.1039/c5nr06882g.
[55] Ferrari AC, Meyer JC, Scardaci V, Casiraghi C, Lazzeri M, Mauri F, et al. Raman spectrum of graphene and graphene layers. Phys Rev Lett 2006;97:1–4. https://doi.org/10.1103/PhysRevLett.97.187401.
[56] Vincent Crist B. Handbooks of monochromatic XPS spectra volume 1 - the elements and native oxides. Handb. Elem. Nativ. Oxides. 1999;1:1–87.
[57] Mizukoshi Y, Oshima R, Maeda Y, Nagata Y. Preparation of platinum nanoparticles by sonochemical reduction of the Pt(II) ion. Langmuir 1999;15:2733–7. https://doi.org/10.1021/la9812121.
[58] Fabish TJ, Schleifer DE. Surface chemistry and the carbon black work function. Proc Electrochem Soc 1984;84:79–109. –5.
[59] Zhou X, Huang X, Qi X, Wu S, Xue C, Boey FYC, et al. In situ synthesis of metal nanoparticles on single-layer graphene oxide and reduced graphene oxide surfaces. J Phys Chem C 2009;113:10842–6. https://doi.org/10.1021/jp903821n.
[60] Tsakova V. Spontaneous carbon-support-induced metal deposition. ACS Omega 2022;7:3158–66. https://doi.org/10.1021/acsomega.1c06225.
[61] Wang L, Gong P, Li W, Luo T, Cao B. Mono-dispersed Ag/Graphene nanocomposite as lubricant additive to reduce friction and wear. Tribol Int 2020;146:106228. https://doi.org/10.1016/j.triboint.2020.106228.
[62] Liu K, Li J, Wang Q, Wang X, Qian D, Jiang J, et al. Designed synthesis of $LaCoO_3$/N-doped reduced graphene oxide nanohybrid as an efficient bifunctional electrocatalyst for ORR and OER in alkaline medium. J Alloys Compd 2017;725:260–9. https://doi.org/10.1016/j.jallcom.2017.07.178.
[63] Zeng G, Li W, Ci S, Jia J, Wen Z. Highly dispersed NiO nanoparticles decorating graphene nanosheets for non-enzymatic glucose sensor and biofuel cell. Sci Rep 2016;6:1–8. https://doi.org/10.1038/srep36454.
[64] Yan X, Li H, Sun J, Liu P, Zhang H, Xu B, et al. Pt nanoparticles decorated high-defective graphene nanospheres as highly efficient catalysts for the hydrogen evolution reaction. Carbon 2018;137:405–10. https://doi.org/10.1016/j.carbon.2018.05.046.